An Improved Azimuth Ambiguity Suppression Method for SAR Based on Ambiguity Area Imaging and Detection

Wen Xuejiao, Qiu Xiaolan, *Senior Member, IEEE*, Cui Lei, Wang Jiyun, and Chen Qi

***Abstract*—In this article, an azimuth ambiguity suppression method based on ambiguity area imaging and detection is proposed, which is suitable for various imaging modes such as strip, spot, and multichannel modes. The basic idea of this method is to focus the image of each azimuth ambiguity area of a single-look complex synthetic aperture radar (SAR) image through a reversible signal processing method, then the strong targets in the focused ambiguity area are detected and eliminated. Finally, the real target image in the main area is obtained through the inverse operation. This method can remove most of the azimuth ambiguity while maintaining the quality of the original image to the greatest extent. In this article, the method of segmentation of complex background and pure background is used to eliminate the error caused by single threshold detection, and the construction of ambiguity area focusing filter in spotlight mode and multichannel mode is studied. This method has good performance in engineering applications. The processing results of real spaceborne SAR images show the effectiveness and validity of the method.**

***Index Terms*—Azimuth ambiguity, signal processing, synthetic aperture radar (SAR).**

I. Introduction

DUE to the specific characteristics of the synthetic aperture radar (SAR) system, peculiar artifacts can appear on SAR images. In particular, finite pulse repetition frequency (PRF) and nonideal antenna pattern give rise to azimuth ambiguity, with the possible presence of "ghosts" on the image. They are due to the replica of strong targets located outside of the antenna main beam, superposed onto low-intensity areas of the imaged scene [1], [13].

Manuscript received 10 May 2022; revised 14 July 2022 and 1 September 2022; accepted 14 September 2022. Date of publication 19 September 2022; date of current version 27 September 2022. This work was supported in part by the National Key R&D Program of China under Grant 2018YFA0701903 and in part by the National Natural Science Foundation of China under Grant 62022082. *(Corresponding author: Qiu Xiaolan.)*

Wen Xuejiao is with the Laboratory of Spatial Information Intelligent Processing System, Suzhou Aerospace Information Research Institute, Suzhou 215000, China, and also with the University of Science and Technology of China, Hefei 230052, China (e-mail: 136037701@qq.com).

Qiu Xiaolan and Cui Lei are with the Laboratory of Spatial Information Intelligent Processing System, Suzhou Aerospace Information Research Institute, Suzhou 215000, China (e-mail: xlqiu@mail.ie.ac.cn; cuilei1167@163.com).

Wang Jiyun is with Suzhou University, Suzhou 215000, China (e-mail: 2727578517@qq.com).

Chen Qi is with the System General Department, China Centre for Resources Satellite Data and Application, Beijing, China (e-mail: chenq_cn@163.com).

Digital Object Identifier 10.1109/JSTARS.2022.3207503

Although most SAR systems are well designed to reduce azimuth ambiguity as much as possible, for targets with very high scattering intensity, it is still difficult to eliminate azimuth ambiguity through system design completely. In addition, during the orbit debugging time of spaceborne SAR, many system parameters are not optimized, and azimuth ambiguity will also appear on the image, affecting the image quality. Therefore, it is urgent to suppress azimuth ambiguity by signal processing without changing the system design.

One of the azimuth ambiguity suppression methods is based on spectrum filtering [2], [3], [4]. This kind of method reduces azimuth spectrum aliasing and then suppresses azimuth ambiguity by spectrum filtering. This kind of method has a limited ambiguity suppression effect and will reduce the azimuth resolution of the image. It uses the way of sacrificing azimuth bandwidth for ambiguity suppression, which has a great impact on the original image. Another kind of method is based on compressed sensing and sparse reconstruction algorithm. Peng et al. [5] realize ambiguity suppression by truncating the Doppler spectrum of the image, then takes the original image as a priori information and the truncated spectrum as the observation result, and iteratively solves the high-resolution image by using a compressed sensing restoration algorithm. This method has low efficiency and is very limited in large scene application. Moreover, the parameters of sparse reconstruction need to be optimized and modified with the image scene, so it cannot deal with the engineering process.

In recent years, some new azimuth ambiguity suppression algorithms have been proposed. Di Martino et al. [6] proposed an azimuth ambiguity suppression method for strip mode based on Chirp-scaling imaging algorithm. Azimuth ambiguities are accurately reconstructed by applying reconstruction filters in the range Doppler and 2-D frequency domain, and then, the reconstructed signal is used for suppressing azimuth ambiguities. This method is mainly used to suppress the azimuth ambiguity of small areas and small targets when the targets in the main area are clear and separable. Application scenarios are limited. Wu et al. [7] proposed an azimuth ambiguity suppression algorithm based on minimum mean square error estimation. It constructs a subspace with low ambiguous power and projects the original image to the aforementioned subspace to suppress the azimuth ambiguity by the minimum mean square error estimation. However, the algorithm needs the help of antenna pattern files, and the amount of calculation is very large, which is not suitable for large scene and azimuth ambiguity with large area. Wu et

al. [8] proposed a method based on spectrum selection and extrapolation. The algorithm selects the subspectra with less ambiguous disturbance and adopts extrapolation with weighted energy measure to obtain a full spectrum. Due to the spectrum extrapolation technology, the azimuth resolution is guaranteed, but at the same time, the noise will be introduced and the image quality will be affected. A method of ambiguity area detection and suppression is proposed in [9]. This article uses ambiguity area imaging to detect and suppress targets in ambiguity area. However, this article does not clearly give the processing methods of different modes, and there is no reasonable expression in detection methods and target suppression. Villano and Krieger [14] present a new method to estimate the local azimuth ambiguity ratio. This article uses the data spectrum and the derived formula and finally applies the constructed filter to detect the azimuth ambiguity ratio. This method mainly detects the azimuth ambiguity ratio of the original image and does not involve the content of azimuth ambiguity suppression.

It can be seen from the above situation that the existing SAR azimuth ambiguity suppression methods are mainly based on the idea of selecting the spectrum with less severe ambiguity for imaging, or based on the idea of sparse reconstruction. However, in fact, due to the ductility of SAR antenna pattern, there may be a serious ambiguity spectrum in a wide frequency band in the main area, and it is difficult to find the area with less serious ambiguity, so the application is limited. In addition, even if the aliased spectrum of some ambiguity areas is suppressed by spectrum filtering, it also affects the spectrum of the main area, reduces the bandwidth and azimuth resolution, further more affects the final image. The sparse reconstruction method is inefficient and will set the weak targets of the scene to zero, which is quite different from the traditional SAR image products and may even affect some applications.

This article proposes an azimuth ambiguity suppression method based on ambiguity area imaging and detection, which can effectively avoid the shortcomings of the above methods. This method can suppress the azimuth ambiguity while preserving the quality of the original image to the greatest extent (not completely without loss). The basic idea is to focus the image of each azimuth ambiguity area of SAR image through a reversible signal processing method, then the strong targets in the focused ambiguity area are detected and eliminated. Finally, the real target image in the main area is obtained through an inverse operation. This method can maximize automation in engineering applications, except for some special scenarios.

The arrangement of this paper is as follows. Section II introduces the causes of azimuth ambiguity and the imaging methods for each order of ambiguity area. Section III introduces the azimuth ambiguity suppression method based on ambiguity area imaging and detection. Section IV gives the experimental processing results of spaceborne data. Section V summarizes the methods proposed in this article.

II. Azimuth Ambiguity Area Focusing Method

A. Causes of Azimuth Ambiguity

Due to Doppler effect, the echo received by SAR can be equivalent to a linear frequency modulation (LFM) signal along the azimuth direction, which is discretized by sampling frequency PRF. In addition, the LFM signal is weighted by the azimuth antenna pattern (AAP). Generally, there are side lobes in the antenna pattern, and the signal at the side lobe is in a relatively high-frequency band. The matched filter used in azimuth compression is usually within the main lobe Doppler bandwidth and the Doppler spectrum where higher than PRF is folded into the azimuth processing bandwidth, which is mixed with the main signal to form azimuth ambiguity. As shown in Fig. 1, the blue dotted line and the yellow dotted line show how the two ambiguity areas folding into the main area.

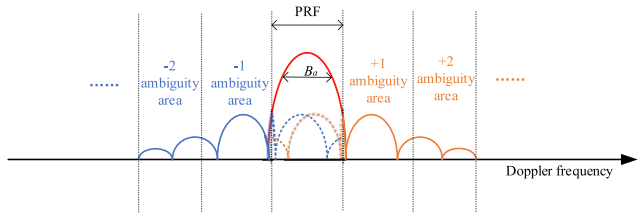

Fig. 1. Schematic diagram of azimuth ambiguity.

When the PRF is high, the signal at the side lobe is very weak relative to the main lobe, so there will be no obvious ambiguity. When the PRF is low, due to the reduction of the sampling rate, the near side lobe of the antenna pattern will produce spectrum aliasing, so that the LFM signal at the side lobe enters the filter bandwidth, resulting in obvious azimuth ambiguity [10]. It can be said that the fundamental reason for azimuth ambiguity is that there are sidelobes in the antenna pattern and the pulse working mode of SAR.

Generally speaking, the side lobe signal of azimuth pattern is folded into the main lobe interval with integer multiple PRF. In this article, we call the signal to obtain the real image as the main lobe signal, call the side lobe signal to obtain the ambiguity image as the ambiguity area signal, and use integer multiple PRF to determine the order of the ambiguity area, as shown in Fig. 1.

The calculation formula of azimuth ambiguity ratio is as follows:

$$AASR = \frac{\sum_{\substack{m=\infty \\ m\neq 0}}^{m=-\infty} \int_{-B_a/2}^{B_a/2} G^2(f_\eta - f_c + mPRF)df_\eta}{\int_{-B_a/2}^{B_a/2} G^2(f_\eta - f_c)df_\eta}. \quad (1)$$

In (1), f_c is the Doppler center frequency, B_a is the azimuth processing bandwidth, $G(f)$ is the AAP, f_η represents the azimuth frequency, and m is an integer and represents the order of azimuth ambiguity area.

According to the definition of azimuth ambiguity ratio given in (1), the main factors affecting azimuth ambiguity are the processing parameters of azimuth imaging and AAP [10].

It should be noted that there is a little difference between strip mode and spotlight mode [11]. For the strip mode, since the direction of the antenna does not change during the synthetic aperture time, the targets with the same slant range and different azimuth positions on the ground travel the same antenna pattern illumination process. As shown in the antenna pattern represented by the black edge line in Fig. 2. Each target in the mapping width has experienced the pattern side lobe irradiation

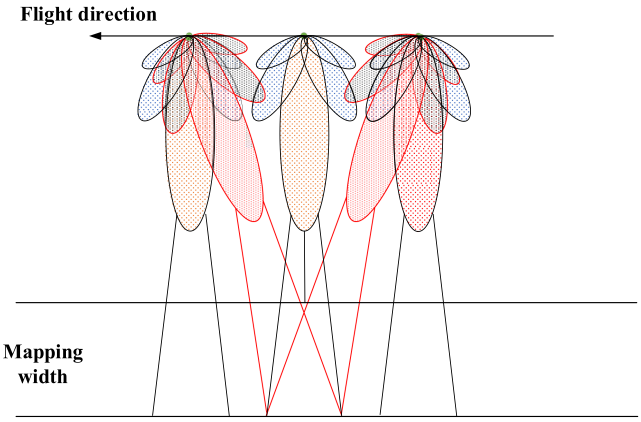

Fig. 2. Working state of strip mode and spotlight mode.

area, the main lobe irradiation area, and then left the main lobe to enter the side lobe irradiation area again. Therefore, the azimuth ambiguity of strip mode target is generally in the form of self-defocusing, that is, the target itself is folded into the main lobe area under the influence of the side lobe. The biggest difference between spotlight mode and strip mode is the change of beam direction. In the strip mode, the antenna beam direction basically does not change. In the spotlight mode, for the imaging area, the radar will constantly adjust its beam direction to ensure that the beam center always points to the center of the imaging area in the whole synthetic aperture time. As shown in the antenna pattern represented by the red edge line in Fig. 2. The target of spotlight mode is generally in the main lobe irradiation area all the time, which makes its side lobe irradiation area change constantly. Therefore, the azimuth ambiguity area is generally expressed as the target of another area different from the target of the main area. This also makes some algorithms that rely on the target characteristics of the main area to calculate and suppress the targets in the ambiguity area invalid.

Excellent system design will make the signal in the ambiguity area as close as possible to the depression of the pattern to reduce the signal energy in the ambiguity area. However, there is also a situation that the system design is insufficient to make the signal in the ambiguity area at the peak of the sidelobe. At this time, the energy of the ambiguity signal becomes larger and the azimuth ambiguity ratio decreases. The ambiguity signal is visible to the naked eye in the image, which greatly affects the image quality.

B. Azimuth Ambiguity Area Focusing

In this article, the azimuth ambiguity is suppressed by focusing on the ambiguity area signal. Therefore, this section mainly describes the focusing method of each order of ambiguity area signal.

The method proposed in this article aims at the single-look complex (SLC) data after imaging, which is obtained by the frequency domain imaging processing algorithm. The flow chart of the signal focusing method in azimuth ambiguity area is shown in Fig. 3. Here are the detailed steps.

1) Azimuth FFT: The azimuth FFT of complex image data can obtain the information in the range Doppler domain. In the

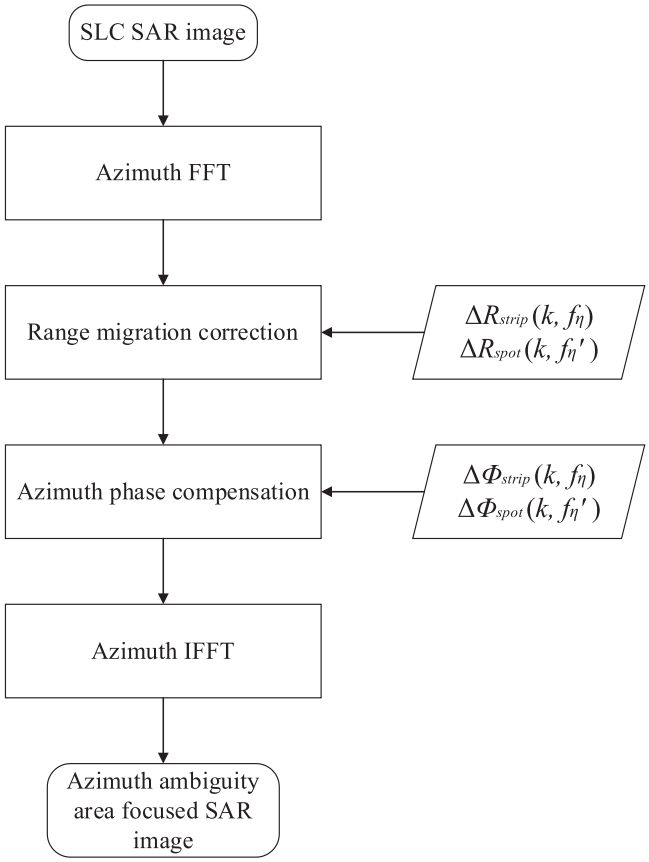

Fig. 3. Flow chart of signal focusing method in azimuth ambiguity area.

range Doppler domain, the range migration of the target in the main area processed by the imaging algorithm has been corrected and its azimuth phase has been compensated.

The range migration of target compensation in the main area is as follows:

$$R_{main}(f_\eta) = \frac{R_{ref}}{\sqrt{1 - \frac{\lambda^2 f_\eta^2}{4V_r^2}}} \tag{2}$$

where R_{ref} is the reference slant range, λ is the wavelength and V_r is the equivalent velocity.

The compensated azimuth phase in the main area is as follows:

$$\phi_{main}(f_\eta) = j\frac{4\pi R_{ref}}{\lambda\sqrt{1 - \frac{\lambda^2 f_\eta^2}{4V_r^2}}}. \tag{3}$$

It should be noted that the azimuth frequency f_η in the formula is generally written as follows:

$$\left(-\frac{PRF_{im}}{2} \sim \frac{PRF_{im}}{2}\right) \tag{4}$$

where PRF_{im} is the azimuth sampling rate in the imaging process, which has different calculation methods in different modes.

For strip mode, the azimuth sampling rate of imaging is consistent with that of the system repetition frequency PRF.

For multichannel mode, the azimuth sampling rate of imaging is the equivalent sampling rate after multichannel synthesis. Assuming that the number of channels is M, the synthetic azimuth sampling rate is M∗PRF.

For spotlight mode, the special imaging geometry of spotlight mode makes its Doppler information different from the general strip mode. The Doppler bandwidth of spotlight SAR consists of two parts, one is the Doppler bandwidth of single point target, and the other is the Doppler center change of targets at different azimuth positions in the same range gate. The total bandwidth of the two is larger than that of the strip mode with the same antenna length. The pulse transmission frequency PRF used in the system design can meet the sampling conditions as long as it is greater than the instantaneous bandwidth, but in fact, the PRF less than the total bandwidth will still cause azimuth aliasing in imaging processing. Therefore, the imaging processing of spotlight mode generally needs to reduce the bandwidth of azimuth echo signal by azimuth deramp processing, so as to reduce the requirement of PRF [12]. Deramp processing mainly removes the change of instantaneous Doppler center of echo with time, so as to reduce the effective bandwidth. At this time, the real Doppler history of the target can be recovered by up sampling the signal in the azimuth frequency domain by filling zero and multiplying time inverse deramp function. Based on the above analysis, a new equivalent PRF named PRF_{new} is generated after spotlight mode imaging, which represents the real Doppler frequency after imaging. Therefore, the azimuth sampling rate is PRF_{new} for the spotlight mode.

In the range Doppler domain, there is also the information of ambiguity signal. The range migration and azimuth phase of signals in each order of ambiguity area are different from those in the main area. In order to focus on the ambiguity area, two steps need to be carried out, which are range migration correction and azimuth phase error compensation.

2) Range Migration Correction of Targets in Ambiguity Area: Taking the k-order ambiguity area signal as an example, which presents the signal mixed into the main area at k times of PRF. The range migration of k-order ambiguity area signal can be obtained as follows:

$$R(k, f_\eta) = \frac{R_{ref}\cos\theta_k}{\sqrt{1-\frac{\lambda^2(f_\eta+k\cdot PRF)^2}{4V_r^2}}} \tag{5}$$

where $\cos\theta_k$ is as follows:

$$\cos\theta_k = \sqrt{1-\left(\frac{\lambda k\cdot PRF}{2V_r}\right)^2}. \tag{6}$$

It should be noted that the PRF here is the system transmission frequency, which is different from the azimuth sampling rate during imaging above named PRF_{im}.

Therefore, it can be obtained that the range migration of k-order ambiguity area signal and main area signal is different as follows:

$$\begin{aligned}\Delta R(k, f_\eta) &= R(k, f_\eta) - R_{main}(f_\eta)\\ &= \frac{R_{ref}\cos\theta_k}{\sqrt{1-\frac{\lambda^2(f_\eta+k\cdot PRF)^2}{4V_r^2}}} - \frac{R_{ref}}{\sqrt{1-\frac{\lambda^2 f_\eta^2}{4V_r^2}}}.\end{aligned} \tag{7}$$

In fact, the range migration of the signal in k-order ambiguity area has a bending of (7) when the imaging algorithm corrects the range migration of the main area signal.

The range migration of k-order ambiguity area can be straightened by range migration correction in range Doppler domain through (7).

3) Azimuth Phase Compensation of Target in Ambiguity Area: We still take the k-order ambiguity area signal as an example, and its azimuth phase error is as follows:

$$\phi(k, f_\eta) = j\frac{4\pi R_{ref}\cos\theta_k}{\lambda\sqrt{1-\frac{\lambda^2(f_\eta+k\cdot PRF)^2}{4V_r^2}}}. \tag{8}$$

It can be obtained that the difference in the azimuth phase error between the k-order ambiguity area signal and the main area signal is as follows:

$$\begin{aligned}\Delta\phi(k, f_\eta) &= \phi(k, f_\eta) - \phi_{main}(f_\eta)\\ &= j\frac{4\pi R_{ref}\cos\theta_k}{\lambda\sqrt{1-\frac{\lambda^2(f_\eta+k\cdot PRF)^2}{4V_r^2}}} - j\frac{4\pi R_{ref}}{\lambda\sqrt{1-\frac{\lambda^2 f_\eta^2}{4V_r^2}}}.\end{aligned} \tag{9}$$

The ambiguity area signal has an azimuth residual phase as shown in (9) when the main area signal is well focused.

After step (2), the azimuth phase compensation is performed on the ambiguity area signal in (9).

4) Azimuth IFFT: After the previous steps, the range migration and azimuth phase of the ambiguity area signal are compensated. At this time, the focused ambiguity area target image can be obtained by using the azimuth IFFT. Of course, at this time, all targets except the targets in the k-order ambiguity area are defocused.

III. Azimuth Ambiguity Suppression Method Based on Ambiguity Area Imaging

In this article, an azimuth ambiguity suppression method based on ambiguity area imaging and detection is proposed for SLC images. A simplified flowchart of the method is shown below.

1) Derivative image generation based on the original SLC image: the derivative images include the imaging results of each ambiguity area, the phase-only image of the original SLC image and the phase-only image of the imaging results of the ambiguity area.
2) Ambiguity area targets detection: selecting the positions of the ambiguity area targets according to the ambiguity area focusing image of the original SLC image.
3) Ambiguity area targets suppression: the phase information of the input data should stay complete and not damaged to keep the integrity of main area signals, which makes it necessary to the use of amplitude suppression for ambiguity suppression.
4) Main area targets reimaging: after suppressing the detected ambiguity area targets, the real image is focused back through the inverse process, so as to obtain the SAR image after azimuth ambiguity suppression.
5) Cycle through all ambiguity areas: set the order of the ambiguity area to be suppressed, and cycle steps 1–4 to suppress the azimuth ambiguity of the specified order.

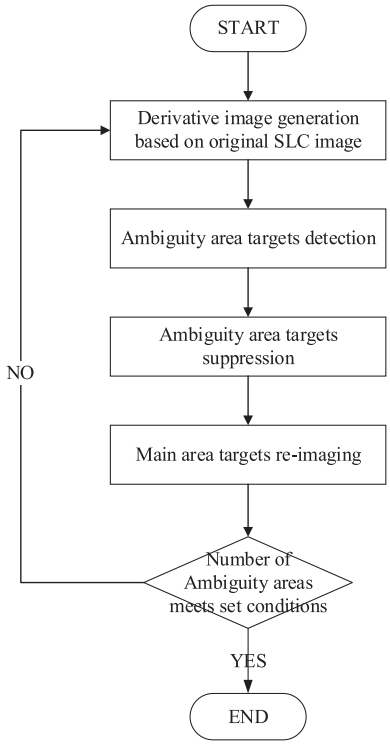

Fig. 4. Flow chart of azimuth ambiguity suppression method.

The following is a detailed step description of the algorithm. The specific steps are described in the following sections (Fig. 4).

A. Derivative Image Generation Based on the Original SLC Image

In order to facilitate the subsequent application of the algorithm, the first step of the algorithm is to generate the required derivative images. Assume that the original SLC image is S_r expressed as

$$S_r = S_r.re + S_r.im \cdot j \tag{10}$$

where $S_r.re$ represents the real part and $S_r.im$ represents the imaginary part, and $j$represents the imaginary units.

The amplitude of S_r is as follows:

$$Asr = \sqrt{S_r.re^2 + S_r.im^2}. \tag{11}$$

Four kinds of derivative images generated based on the original image are introduced below, along with the generation flowchart shown in Fig. 5.

1) Ambiguity area focused image based on original SLC image

This image is obtained from the ambiguity area imaging of the specified order of S_r (the original SLC image) through the method described in Section II-B. The image is recorded as S_{r_am} expressed as

$$S_{r\_am} = S_{r\_am}.re + S_{r\_am}.im \cdot j \tag{12}$$

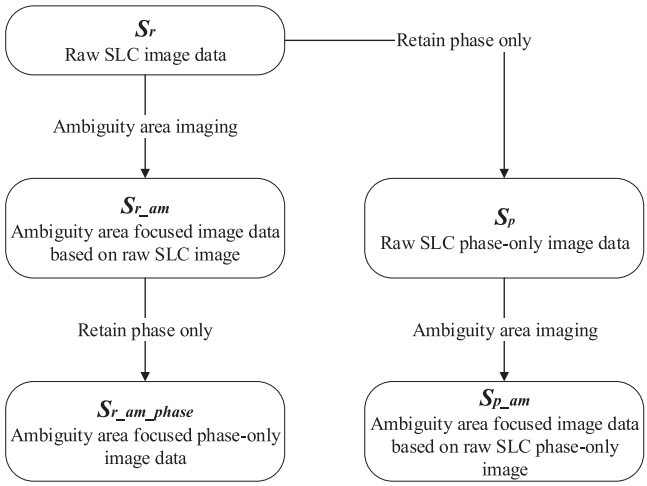

Fig. 5. Flow chart of derivative images generated based on the original image.

where $S_{r\_am}.re$ represents the real part and $S_{r\_am}.im$ represents the imaginary part. The amplitude of S_{r_am} is

$$Asr\_am = \sqrt{S_{r\_am}.re^2 + S_{r\_am}.im^2}. \tag{13}$$

2) Phase-only image data of the ambiguity area focused image

This image is obtained from taking only phase result of the S_{r_am} (ambiguity area focused image based on original SLC image) which is recorded as $S_{r\_am\_ph}$ expressed as

$$S_{r\_am\_ph} = \frac{S_{r\_am}.re}{Asr\_am} + \frac{S_{r\_am}.im}{Asr\_am} \cdot j. \tag{14}$$

3) Phase-only image data of original SLC image

This image is obtained from taking only phase result of the S_r (original SLC image) which is recorded as S_p expressed as

$$S_p = \frac{S_r.re}{Asr} + \frac{S_r.im}{Asr} \cdot j. \tag{15}$$

4) Ambiguity area focused image data based on phase-only image data of original SLC image

This image is obtained from the ambiguity area imaging of the specified order of S_p (phase-only image data of original SLC image) through the method described in Section II-B. The image is recorded as S_{p_am} expressed as

$$S_{p\_am} = S_{p\_am}.re + S_{p\_am}.im \cdot j. \tag{16}$$

B. Ambiguity Area Targets Detection

Traditional methods, as described in [9], mainly use the threshold method to detect ambiguity area in image S_{p_am}. This method sets a single threshold to screen out the targets in the ambiguity area, which has limitations. When the threshold is set too high, the method will miss most of the targets in the ambiguity area. On the contrary, when the threshold is set too low, the method will screen out the targets in the main area, resulting in the energy loss of the targets in the main area and quantitative top cutting phenomenon.

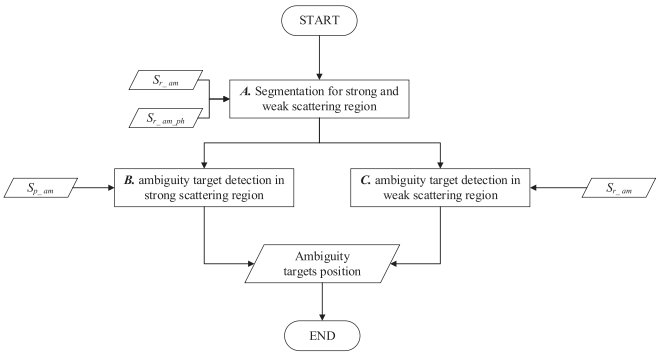

Fig. 6. Flow chart of ambiguity area target detection method.

In the experiment, we found that only a single threshold detection for the image S_{p_am} needs a reasonable threshold, which can hardly be found. When the threshold is too high, the azimuth ambiguity in the weak scattering region of the original image will not be detected, resulting in a limited ambiguity suppression effect. When the threshold is too low, targets in the strong scattering area of the original image will be detected as azimuth ambiguity, resulting in the energy loss of the target in the main area and the deterioration of the imaging result.

In view of this situation, this article proposes a new method. First, the scene is segmented to obtain two regions. The first part includes the position where there is no azimuth ambiguity and the position where the azimuth ambiguity energy is far less than the background energy, which is called the strong scattering region; The second part contains the position where the azimuth ambiguity energy is much greater than the background energy, which is called the weak scattering region. Second, the target in ambiguity area is detected for the two regions respectively. For the strong scattering region, we still use a single threshold for detection in image S_{p_am}. At this time, the threshold can be set higher to reduce the false detection rate of the target in the main area. For the weak scattering region, the image S_{r_am} is used for CFAR detection to screen the targets in the ambiguity area in the weak background.

The flow chart of the ambiguity area target detection method in this article is shown in Fig. 6.

The detailed steps are as follows.

1) Segmentation for Strong and Weak Scattering Region: We know that image contrast is a tool that can describe image quality and information. For a 2-D image, its image contrast *Con* is defined as

$$E_1 = E(S^2)$$
$$E_2 = [E(S)]^2$$
$$Con = \frac{E_1}{E_2} \tag{17}$$

where $E(\sim)$ represents the mean value, and S represent the sum of the amplitude of the data.

Image contrast reflects the concentration of image pixel distribution. Generally, the better the image focusing effect, the higher the contrast.

However, it is not enough to divide the strong and weak scattering regions only by calculating the contrast in one image. The selection of threshold will lead to segmentation error. Therefore, a method of strong and weak scattering region segmentation combining the original image and phase-only image is proposed in this article.

In fact, the process of taking the phase of a complex image is to set all the amplitudes of the image to 1 that will reduce the contrast of the image. The degree of contrast decline depends on the contrast in the original image. If the intensity contrast in the original image is obvious such as the azimuth ambiguity of the urban area on the sea surface, the amplitude normalization will get a large contrast change value; on the contrary, if the intensity contrast in the original image is not obvious, such as the pure sea surface without ambiguity and complex scenes with little azimuth ambiguity, the amplitude normalization will get a relatively small contrast change value.

Therefore, it can be concluded that the contrast of weak scattering region declines more in the process of phasing. Based on this conclusion, this article divides the strong and weak scattering regions by comparing the contrast decline of image data S_{r_am} and image data $S_{r\_am\_ph}$. The main steps are as follows.

1) To obtain image result of certain ambiguity area S_{r_am} and the corresponding phase-only image result $S_{r\_am\_ph}$.
2) To set the sliding window size $W * W$ (range direction $*$ azimuth direction) and the segmentation threshold T_s.
3) To calculate the contrast decline result of S_{r_am} and $S_{r\_am\_ph}$ in the sliding window, expressed as $EP_{\_am}$ and $EP_{\_ph}$.
4) To compare the contrast decline result with the segmentation threshold T_s. If $EP_{\_am}$ (or $EP_{\_ph}$) $< T_s$, it is considered a strong scattering region, otherwise it is considered a weak scattering region.
5) To obtain the segmentation result of the whole image by adjusting the sliding window position covering the whole image.

It should be noted that the three images (S_{r_am}, $S_{r\_am\_ph}$, S_{p_am}) are the imaging results of ambiguity area, which are only distinguished in amplitude, and their relative positions do not change. Therefore, the final segmentation result obtained in this section is expressed in position coordinates. The strong scattering region is recorded as P_s and the weak scattering region is recorded as P_w.

The correctness of segmentation is very important. Assuming that the size of the image is $N_a * N_r$ and the size of the sliding window is $W*W$, the image can be roughly divided into $A*R$ blocks. By comparing the contents of each block to determine whether it is correctly divided into strong / weak scattering areas. Assuming that the number of blocks correctly divided is N_y, the accuracy of segmentation is

$$A_{rate} = N_y / A \cdot R \cdot 100\%. \tag{18}$$

2) Ambiguity Target Detection in Strong Scattering Region: The energy of the ambiguity area targets in the strong scattering region is weak and difficult to distinguish in the image S_{r_am}. In order to make the targets of the ambiguity area more obvious, this

article mainly focuses on the detection and processing of image S_{p_am}. It is mentioned in [9] that after phasing the original image and then imaging the ambiguity area, the ambiguity area image can be more prominent from the main area background.

If the refocusing process is applied directly to the original SAR image, the ambiguity signal of the strong true targets often exceeds the focused ambiguity signal and disturbs the detection of the focused ambiguity signal. On the other hand, if we discard the amplitude and apply refocusing process to the phase-only image, there is more chance for the focused ambiguity signal to exceed the blurred true target signal.

The detection method in [9] is threshold screening, but it does not specify the selection method of the threshold. Considering that the amplitude of the phase-only image S_p is 1, the energy of the target in the ambiguity area is enhanced and the energy of the target in the main area is weakened after the ambiguity area focusing on image S_{p_am}, this article mainly selects the threshold from the distribution of pixel values.

The steps of the overall strong scattering region ambiguity target detection method are as follows.

1) To obtain the ambiguity area focusing result of the original phase-only image data S_{p_am} and extract the strong scattering region according to the P_s position information.
2) To set the threshold T_k: sorting all pixel values with amplitude greater than 1 from large to small and taking the pixel value at 30% position as the threshold.
3) To compare the pixel amplitude K_{ij} in the region with the threshold T_k. If $K_{ij} > T_k$, it is considered as ambiguity target, and the position is recorded as P_{s_Am}, otherwise it is considered as the main area, and the position is marked as P_{s_main}.

3) Ambiguity Target Detection in Weak Scattering Region: In weak scattering region, such as forest land and water area, the ambiguity targets are obvious with no need to be detected on the phase-only ambiguity focusing image S_{p_am}. In [9], the strong and weak scattering regions are not distinguished, which will lose the advantages of good contrast and easy detection of the weak scattering region itself. In this article, the weak scattering area is divided separately, and the problem of ambiguous area target detection in the image S_{r_am} can be translated into the detection of strong backscattering targets under weak background, which is normally solved by a target detecting algorithm called CFAR.

In this article, we choose the double-parameter CFAR detection algorithm to achieve the detection of main ambiguous area targets. This algorithm sets up three sliding windows as shown in Fig. 7 and realizes the target detection by comparison of the pixel grayscale in the target window and the self-adapting threshold, which is acquired by false alarm rate (*PFA*) and background clutter modeling, which is assumed to be Gaussian distribution with mean value μ and standard deviation σ in the background window.

The specific steps are as follows.

1) Set up for the length of sliding windows

The size of the general target window should be the same as the minimum size of targets to be detected. The length of the protection window is generally twice the maximum target size, while the background window being selected as two or four times the protection window size. The step length of the sliding window is in accordance with the size of the target window. The ambiguous area image is usually an integrated area composed of strong scattering points, different from ships that have a uniform shape, making it necessary to do some experiments to determine the reasonable length of the three windows.

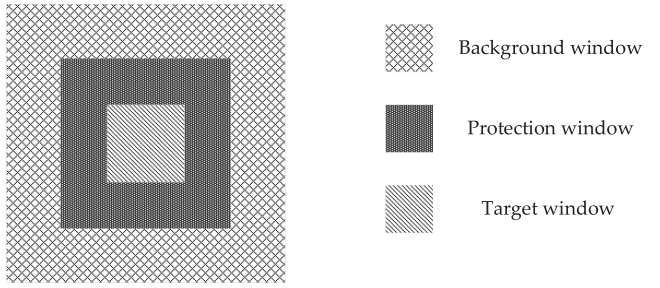

Fig. 7. This is a figure that shows the geometric relation of three sliding windows. They are all squares and the inside is the target window, the middle is the protection window, and the outside is the background window.

2) Calculation of threshold including μ and σ for the background window

To set the detection threshold *T*, we need the distribution function of background clutter and the given *PFA*. Supposing $\Phi(\cdot)$ presents the Gaussian distribution function, we can get the following expression:

$$\begin{aligned} T &= \sigma \times t_1 + \mu \\ t_1 &= \Phi^{-1}(1 - PFA) \end{aligned} \tag{19}$$

where μ and σ are calculated according to each background window, making the threshold *T* changing adaptively. In fact, the background clutter may not be in conformity with the standard Gaussian distribution absolutely, forcing us to determine the reasonable choice of t_1 through experiments.

3) Target detection

If the gray value of a pixel in the target window is I_{tar}, then the target detection criterion is as follows:

$$I_{tar} > \sigma \times t_1 + \mu. \tag{20}$$

As mentioned above, we need some experiments to determine the reasonable parameters of the algorithm. Limited to the characteristics of the ambiguous area image itself, this method cannot evaluate the detection quality by the specific quantity of right detecting targets. We can only find a comparatively good value interval by comparing the results from visual observation.

Through CFAR detection, the positions of the ambiguity target in the weak scattering region are recorded as P_{w_am}, and the opposite positions are recorded as P_{w_main}.

It should be noted that the threshold and other parameters used in segmentation and detection in this article are empirical values, that is, the basic values obtained after many experiments, and do not have uniqueness. QL-01 provides a large number of azimuth ambiguity data (dozens) in the early stage in orbit for this study (now, the satellite no longer has the problem of high azimuth ambiguity after subsequent adjustment). A large number of data cover many typical scenes, so this article adds some simulation

experiments on the basis of the actual data, and then obtains the empirical values of a series of parameters in this method. According to the parameters set in this article, more than 90% of the data can automatically complete the azimuth ambiguity suppression.

4) Definition of Detection Rate and False Detection Rate: The detection targets of this method are continuous discrete strong point target cluster, so it cannot give the same detection rate, false detection rate, and false alarm rate as ship detection.

This article redefines a new detection rate and false detection rate. It is tedious and unrealistic to evaluate the detection rate based on the pixel level, so we choose the block-based method to calculate the detection rate and the false detection rate. We set the block size as *DA*∗*DR*, and the whole graph is divided into *SA*∗*SR* blocks.

- Calculation of truth value: in the image to be detected, the blocks containing the focused ambiguity area target are considered as the true value of ambiguity detection, and can be manually counted. The number of blocks with the true value is defined as *N_true*. This set is defined as *S_true*. Other blocks that do not contain the target of the focused ambiguity area are considered false value, and the number of blocks with false value is defined as *N_false*. This set is defined as *S_false*.
- Calculation of detection value: in the image of the detection result, the blocks with detection targets in the blocks included in the set *S_true* are considered as the blocks that have been successfully detected, and can be manually counted. The number of blocks with detection values is defined as *N_detect*.
- Calculation of false detection value: in the image of the detection result, the blocks with detection target in the blocks included in the set *S_false* are considered as false detection, and can be counted manually. The number of blocks with a false detection value is defined as *N_error*.

Therefore, the detection rate can be defined as

$$T_{rate} = \frac{N\_\text{detect}}{N\_\text{true}} * 100\%. \tag{21}$$

The false detection rate can be defined as

$$F_{rate} = \frac{N\_\text{error}}{N\_\text{false}} * 100\%. \tag{22}$$

The detection rate and false detection rate defined above can explain the correctness of the detection method in this article.

5) Applicable Scenarios of This Method:

1) The strong and weak scattering scenes have obvious contrast and are easy to segment

According to our previous definition of strong and weak scattering scenes, we can see that strong scattering scenes are actually scenes with complex backgrounds, and weak scattering scenes are actually scenes with pure backgrounds.

The images with obvious contrast between strong and weak scattering scenes are easy to separate and then we can use different targeted methods to detect the ambiguity areas respectively. This can greatly reduce the missed detection rate and false detection rate. But at the same time, it should be noted that for scenes that are not easy to be segmented from strong and weak scattering scenes, once the scenes with complex background and pure background cannot be processed separately, the detection results of ambiguity areas are prone to errors, which is also one of the limitations of this method.

2) Discrete distribution ambiguity targets in strong scattering scenes (i.e., scenes with complex backgrounds)

For scenes with complex backgrounds, we use the ambiguity area focused result of phase-only image for detection. In this image, the amplitude of the complex background should be less than 1, and the amplitude of the focused ambiguity target should be enhanced, which is related to the degree of defocus. The greater the degree of defocus, the higher the increase of its amplitude after refocusing making it easier to stand out from the complex background with an amplitude less than 1.

But in the meantime, it should be noted that the threshold detection method is used for the detection of such scenes. In order to prevent the impact on the main area targets, the threshold will generally be set higher, so some ambiguity area targets whose amplitude does not increase significantly after focusing will be missed. In addition, if the target focused in the ambiguity area covers the position of the target in the main area, there will inevitably be false detection which can cause the energy loss of the target in the main area. This is also one of the limitations of this method.

3) Ambiguity targets with large energy in weak scattering scenes (i.e., scenes with pure backgrounds)

For the scene with pure background, we adopt the detection method of CFAR, which is suitable for detecting relatively independent strong targets in weak background, such as ship targets in the sea, which are often detected by CFAR. Therefore, the targets in the ambiguity area detected in the weak background in this article should be relatively independent strong targets. There are limitations in the detection of distributed targets with wide distribution and low energy.

C. Ambiguity Area Targets Suppression

The phase information of the input data should stay complete and not damaged to keep the integrity of main area signals, which makes it necessary to the use of amplitude suppression for ambiguity suppression. We divided the image result S_{r_am} into two parts according to the detection result

$$S_{r\_am}(x,y) = \sum_{x,y \in P_{s\_am} and P_{w\_am}} S_{r\_am}(x,y) + \sum_{x,y \notin P_{s\_am} and P_{w\_am}} S_{r\_am}(x,y). \tag{23}$$

The amplitude of the detected pixel is reduced by *N* times, and we can get the result as

$$S_{r\_su}(x,y) = \sum_{x,y \in P_{s\_am} and P_{w\_am}} S_{r\_am}(x,y)/N + \sum_{x,y \notin P_{s\_am} and P_{w\_am}} S_{r\_am}(x,y). \tag{24}$$

The extent of suppression is an alternative to manual input. Generally, we choose the attenuation multiplier N for the aim that ambiguous signal power lower than main area power after standard imaging by 0–5 dB.

Here we need to pay attention to two unexpected situations.

1) The detected ambiguity area targets contain the main area target, that is, there is a false detection. At this time, the energy of the targets in the main area will be reduced together causing energy loss.
2) Some targets in the ambiguity area are not detected, that is, there is missed detection. At this time, the targets in this part of the ambiguity area are not suppressed, and will still exist in the final image.

In order to prevent the above phenomena, we should pay more attention to the limitations of this paper when detecting targets.

D. Main Area Targets Reimaging

The acquisition process of S_{r_am} is detailed in Section II, which is reversible. Therefore, the ambiguity suppression result of the original image can be obtained by the inverse operation of ambiguity area imaging. The inverse operation is performed on the image S_{r_su} in the previous section, including azimuth FFT, azimuth phase inverse compensation, range migration inverse correction and azimuth IFFT.

In addition, this method will carry out cyclic processing for the 1–3 order ambiguity area. For each order of ambiguity area targets, imaging, detection, and ambiguity suppression for the detection area will be carried out to obtain the suppression results of each order of ambiguity area.

In order to evaluate the effect of ambiguity suppression, we measured the intensity of azimuth ambiguity before and after suppression in the same area, so as to achieve the purpose of quantitative evaluation of azimuth ambiguity suppression.

IV. Experimental Results

A. Processing Results of Large Scene

This method was originally developed for QL-01 satellite. Because the parameters had not been adjusted to the best, there was a large area of azimuth ambiguity in the initial stage of QL-01 satellite in orbit (the data quality of the satellite has been improved now). How to remove the azimuth ambiguity quickly, effectively, and automatically is the top priority of this study. Therefore, this method has its advantages in removing large-area azimuth ambiguity.

This section selects the images taken by QL-01 satellite during one week in orbit. The image was taken in Dubai in strip mode. The original image is shown in Fig. 8(a). It can be seen that there is serious azimuth ambiguity in the image.

Firstly, we get the $+1$ ambiguity area imaging result which is shown in Fig. 8(b). It can be seen that ambiguity area targets are mixed together with the strong scattering region while clearly visible in the weak scattering region.

The white part in Fig. 8 indicates the range direction and azimuth direction of the image. Unless otherwise specified, the direction annotation in subsequent images is the same. There is

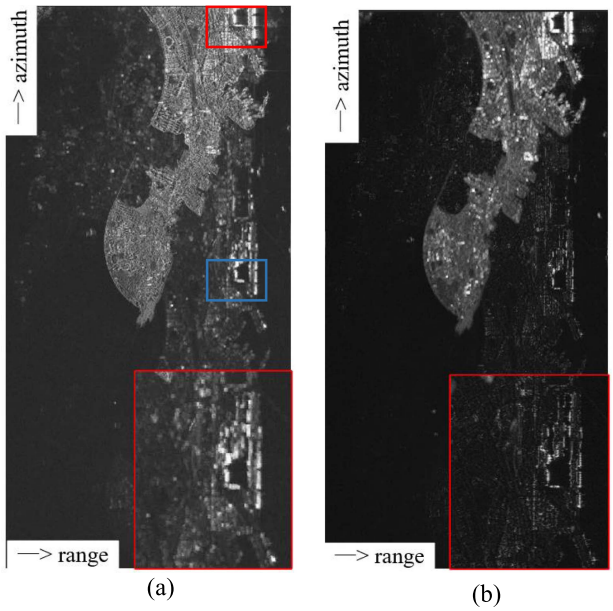

Fig. 8. Original image result and the ambiguity area imaging result. (a) Original image result. (b) $+1$ ambiguity area image result.

Fig. 9. Segmentation results of strong and weak scattering regions.

a local enlarged image in the lower right corner of the image in Fig. 8(a) and (b), which can show the effect of focusing ambiguity area targets.

The contrast reduction threshold in the strong and weak scattering segmentation method is set to 2.1, and the sliding window size is set to $64 * 64$. For the scene of land sea junction as shown in Fig. 8(a), we set the threshold to 2.1 through many experiments (including real data and simulation data). In fact, this is an empirical value, not unique. The segmentation results of strong and weak scattering regions are shown in Fig. 9, where the black part represents weak scattering regions and the white part represents strong scattering regions. By comparing

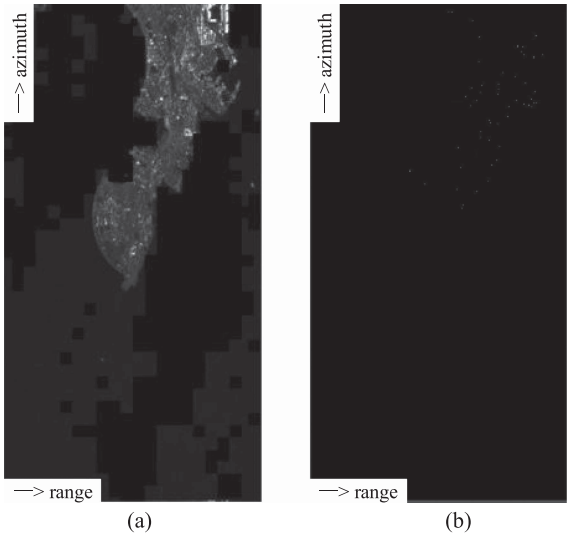

Fig. 10. Detection results of strong scattering regions. (a) Ambiguity imaging result. (b) Detection result of (a).

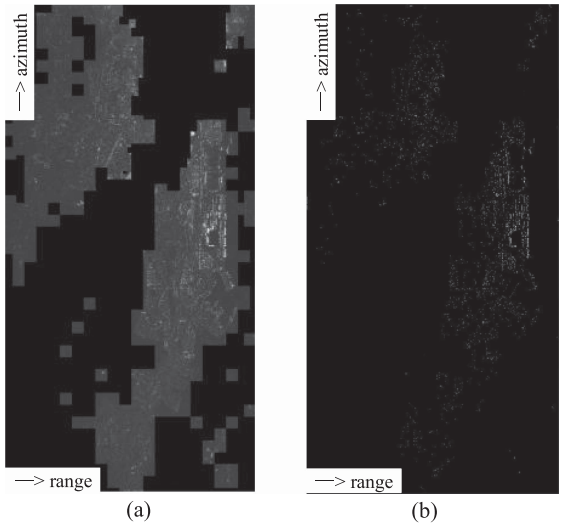

Fig. 11. Detection results of weak scattering regions. (a) Ambiguity imaging result. (b) Detection result of (a).

Figs. 8(a) and 9, we get the accuracy of more than 90% through (18). The black part corresponds to the sea part with ambiguity (low scattering area) in the original image, and the white part corresponds to the land part and sea part with no ambiguity (strong scattering area) in the original image.

Based on the segmentation results, we detect the ambiguity area targets for the two parts respectively.

The image used for strong scattering region detection is S_{p_am}, the result of the strong scattering area in the image is shown in Fig. 10(a). Since the amplitude of the background clutter is less than 1 for phase-only image, the amplitude of ambiguity area after focusing should be enhanced. Therefore, according to many experiments on the focusing effect of the ambiguity area of the complex background, the threshold is set to 2.3. The detected targets in the ambiguity area are shown in Fig. 10(b). The azimuth ambiguity of this data on land is basically absent, so the detected results are not obvious.

The image used for weak scattering region detection is S_{r_am}, the result of the weak scattering area in the image is shown in Fig. 11(a), and the ambiguity area target detection result obtained after CFAR detection is shown in Fig. 11(b). Compared with Fig. 11(a) and (b), it can be seen that most ambiguity area focusing targets have been detected.

Indeed, the parameters of CFAR cannot be set completely automatically. We have determined a set of detection parameters based on many detection experiments of strong targets in weak background. In practical application, it can cope with most scenarios, but if you want to obtain more accurate detection results, you still need to do specific analysis for specific data. Our goal is to remove large areas of azimuth ambiguity, so we have tolerance for some missed detection and false detection.

We combine the ambiguity area targets detected in the strong and weak scattering area to obtain the overall ambiguity area detection results, as shown in Fig. 12(a), and then apply the method proposed in [9] to detect the ambiguity area targets. The result is shown in Fig. 12(b) and (c). (b) represents the high threshold and (c) represents the low threshold. It can be seen that the method in [9] misses the ambiguity area targets in many sea areas when the threshold is set too high and screens out many targets in the main area incorrectly when the threshold is set too low. The results show that the method proposed in this article is more accurate for detecting ambiguity area targets.

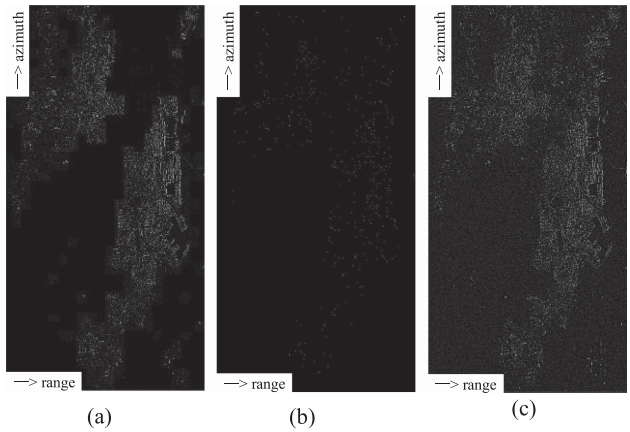

Fig. 12. Ambiguity area detection results of different methods. (a) Detection result of this article's method. (b) Detection result of [9] method with high threshold. (c) Detection result of [9] method with low threshold.

TABLE I
RESULTS OF DETECTION RATE AND FALSE DETECTION RATE

item	Fig.12(a)	Fig.12(b)	Fig.12(c)
Detection rate	98.8%	56.7%	100%
False detection rate	4.6%	2.4%	62.5%

According to the detection rate and false detection rate defined in (21) and (22), we calculate the indexes of the three detection images in Fig. 12 as shown in Table I. It can also be seen from

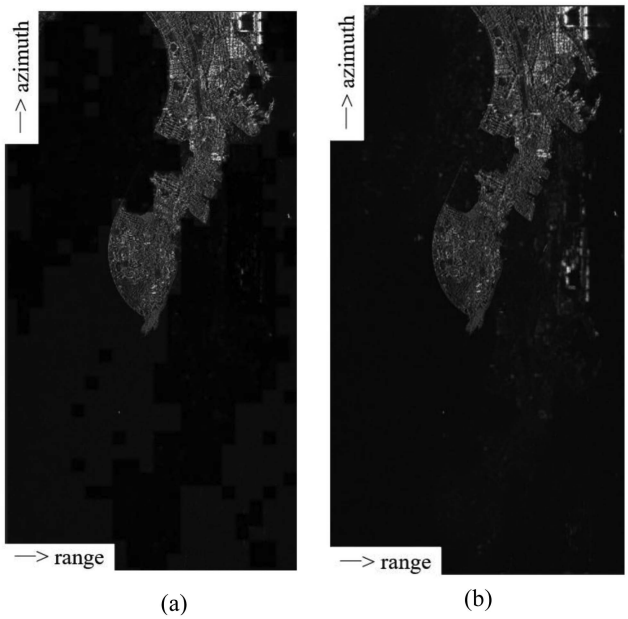

Fig. 13. Ambiguity suppression result of Fig. 8(a). (a) Ambiguity suppression result of this article's method. (b) Ambiguity suppression result of [9]'s method.

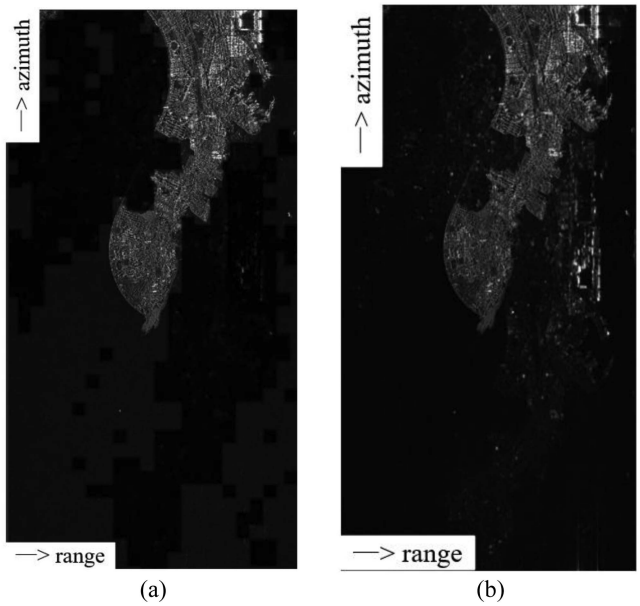

Fig. 14. Ambiguity suppression result of Fig. 8(a). (a) Ambiguity suppression result of this article's method. (b) Ambiguity suppression result of [6]'s method.

TABLE II
RESULTS OF AZIMUTH AMBIGUITY SUPPRESSION

item	Raw image	Method of this article	Method of [9]	Method of [6]
Ambiguity ratio (dB)	-10.8676	-29.4615	-13.3261	-14.5434
Ambiguity area average energy (dB)	23.6488	5.0549	21.1903	19.9730

the results in the table that the method in this article maintains a high detection rate and a low false detection rate compared with [9].

We set the suppression intensity N as 60 dB. The azimuth ambiguity suppression result of this method is shown in Fig. 13(a). The azimuth ambiguity suppression result of [9] is shown Fig. 13(b).

In Fig. 8(a), the part in the red box is the main area target, and the part in the blue box is the ambiguity area target. We find the corresponding positions in Fig. 13(a) and (b), respectively, and calculate the ambiguity ratio. The results are listed in Table II. We also calculated the average energy of the ambiguity area of the raw image, the method in this article and the method of reference [9], and the results are also listed in Table II. It can be seen that the azimuth ambiguity ratio of this method decreases significantly, which indicates that the azimuth ambiguity is basically invisible in the image. Through comparison, we can also see that the azimuth ambiguity suppression effect of this method is better.

In addition, we compare the spectral filtering method of [6]. The processing results of this method are shown in Fig. 14(b) and the statistical results of azimuth ambiguity ratio are listed in Table II. It can be seen that the ambiguity suppression effect of this article's method is better than that proposed in [6]. In fact, the method in [6] relies on accurate imaging parameters and AAP to construct a perfect filter. The antenna pattern provided by the QL01 satellite data in this article may not be accurate. Compared with the method in [6], the method in this article is more flexible while it does not need other data other than imaging parameters.

B. Processing Results of Complex Background

In order to verify the processing effect of this algorithm in complex background, this section selects the images taken by QL-01 satellite during one week in orbit. The image was taken in Istanbul in spotlight mode. The raw image is shown in Fig. 15 with serious azimuth ambiguity, covering the whole image. The ground feature information of the real image is covered under the azimuth ambiguity. Azimuth ambiguity and real ground objects are intertwined.

The reason why we think these interferences are azimuth ambiguity is mainly because the corresponding main area image can be found in the image. In Fig. 15, the red box is the main area image, and the blue box is the corresponding ambiguity area image.

We intercepted a small piece as the experimental object, as shown in Fig. 16(a). The azimuth ambiguity focusing result based on the phase-only image is shown in Fig. 16(b). The 3-D diagram is shown in Fig. 16(c). It can be seen that the intensity of the target in the ambiguity area is significantly higher than that of the background clutter.

We set the threshold to 2.3, and the detected targets in the ambiguity area are shown in Fig. 17(a). According to the definition

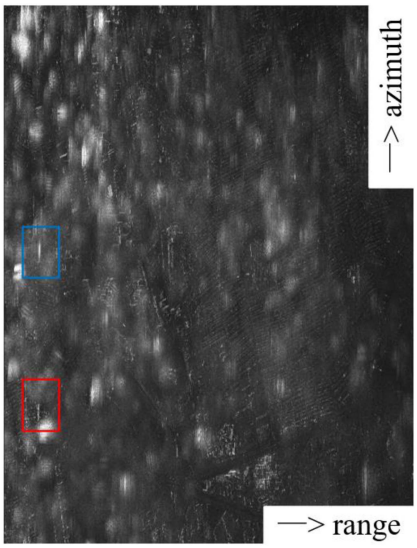

Fig. 15. Original image result of QL-01 taken in Istanbul in spotlight mode.

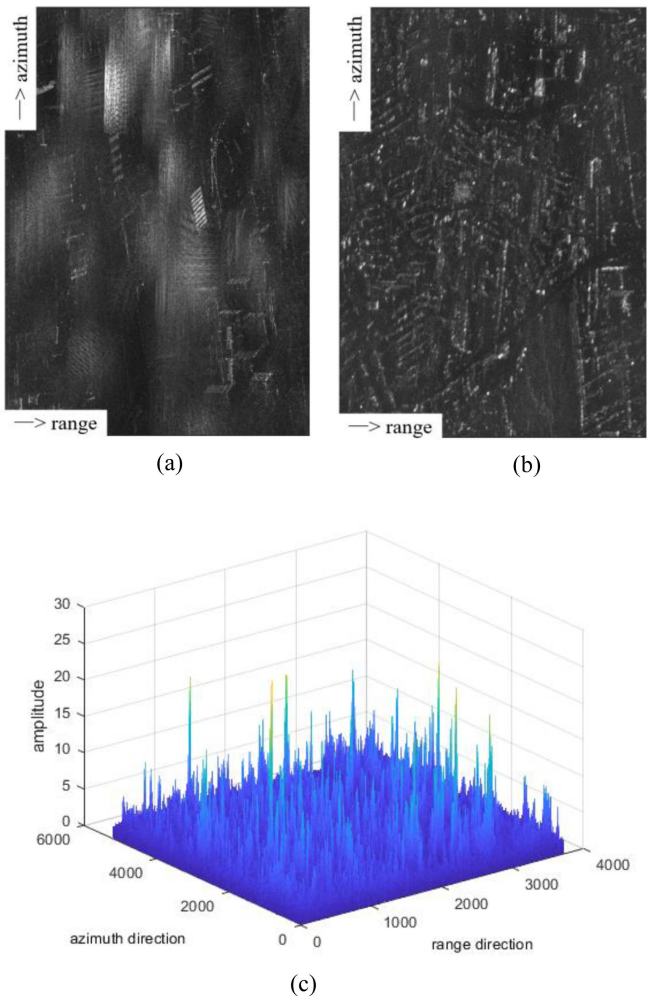

Fig. 16. Focusing results of ambiguity area for slice data of QL-01 taken in Istanbul. (a) Image of slice data. (b) Ambiguity focusing result of the phase-only image. (c) 3-D diagram of ambiguity focusing result.

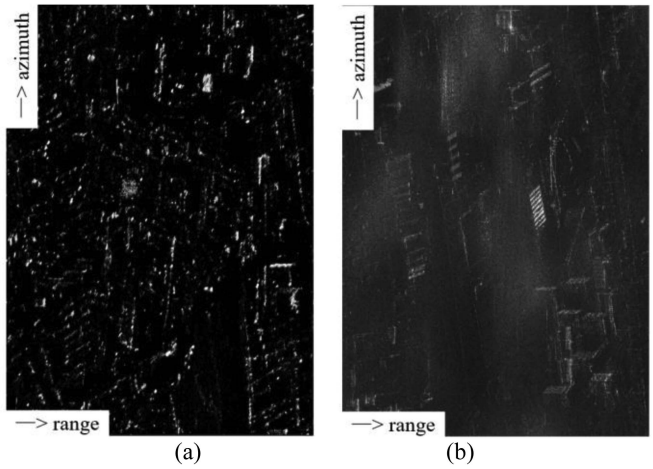

Fig. 17. Detecting and ambiguity suppression results of the slice data. (a) Detecting result (b) Ambiguity suppression result.

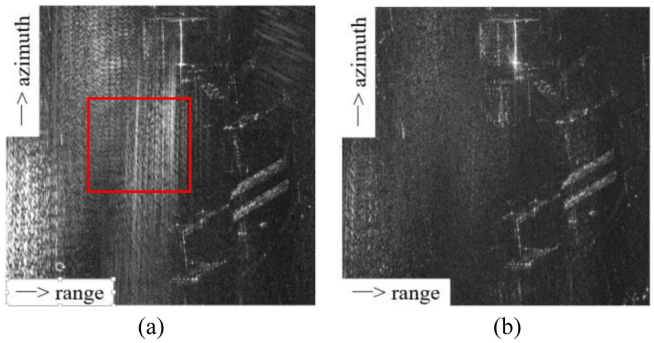

Fig. 18. Comparison before and after ambiguity suppression of local enlarged image. (a) Local enlarged image of raw data. (b) Local enlarged image of ambiguity suppression data.

in (21) and (22), we calculate the detection rate of Fig. 17(a) as 89.8%, the false detection rate as 4.2%. Due to the low energy of some ambiguity areas, the amplitude has not been significantly improved after focusing, so there is a certain degree of missed detection. At the same time, due to the complex background, the defocusing energy of some main areas is mixed with the energy of ambiguity areas, and there is a certain amount of false detection.

The result of ambiguity suppression is shown in Fig. 17(b). Comparing Figs. 16(a) and 17(b), it can be seen that most of the azimuth ambiguity has been suppressed. The main area targets covered by azimuth ambiguity can also be seen. Due to the missed detection, there are still a small number of azimuth ambiguity residues, which are mainly distributed with weak energy.

We take the local enlarged images of Figs. 16(a) and 17(b), as shown in Fig. 18. Through comparison, we can see that most of the azimuth ambiguity has been removed, leaving a part of the distributed ambiguity with weak energy. Due to false detection, the strong target in the main area has a certain degree of roof cutting phenomenon, but it does not affect the visual effect.

Since it is difficult to find the target in the main area corresponding to the ambiguity target, we only calculate the average

TABLE III
RESULTS OF AZIMUTH AMBIGUITY SUPPRESSION

item	Raw image	Method of this article
Ambiguity area average energy (dB)	41.1079	35.4455

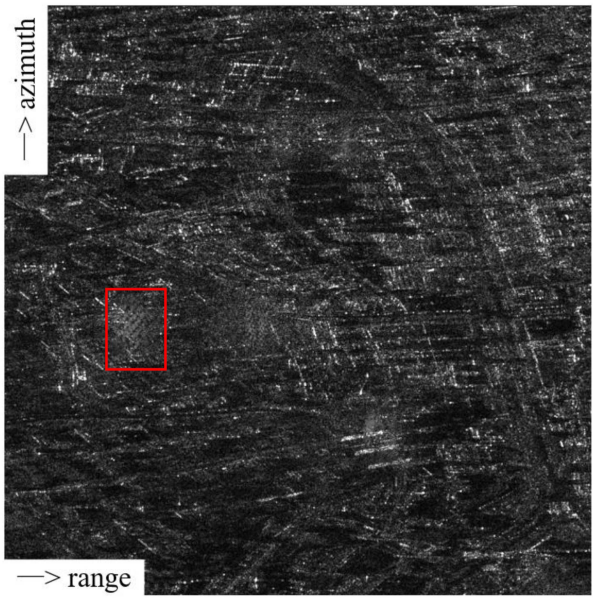

Fig. 19. Original image result of QL-01 taken in Roma in strip mode.

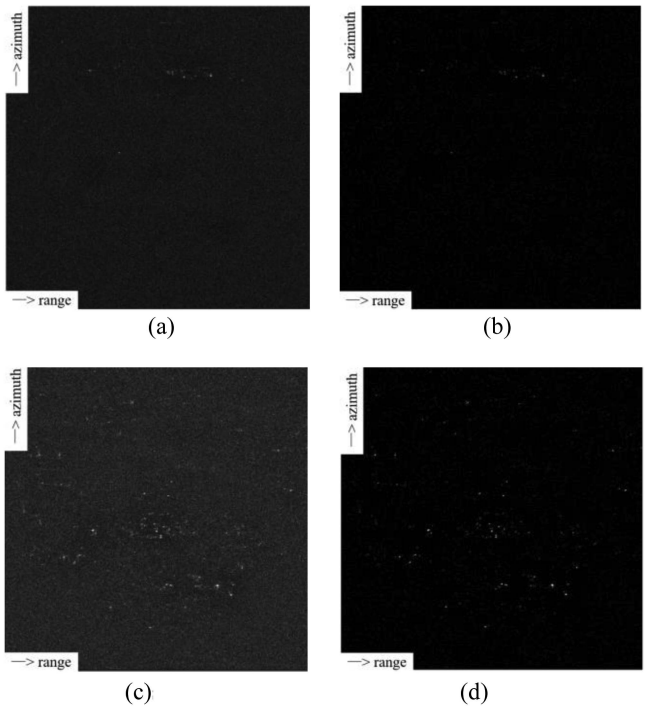

Fig. 20. Focusing and detecting results of the ambiguity area for slice data of QL-01 taken in Roma. (a) First-order ambiguity area focusing result. (b) Detection result of (a). (c) Second-order ambiguity area focusing result. (d) Detection result of (c).

energy of the ambiguity area to evaluate the effect of ambiguity suppression. The objectives used for the assessment are from the parts circled in the red box in Fig. 18(a). The results are listed in TABLE III. It can be seen from the results that the energy value of the ambiguity area decreases, which shows the feasibility of this method.

In addition, we selected an image in strip mode as shown in Fig. 19. The background of the main area of the image is complex, and the target energy in the ambiguity area is weak. In fact, the method in this article has advantages in dealing with this kind of scene, because the imaging results in the ambiguity area of the phase-only image are more prominent.

Fig. 20 shows the imaging result of $+1$ order and -1 order azimuth ambiguity of the image and the corresponding detection results. The detection rate of $+1$ order is 99.5% and the false detection rate is 1.4%. The detection rate of the -1 order is 98.5%, and the false detection rate is 2.6%. It can be explained that the detection result of the ambiguity area is relatively accurate. Fig. 21 shows the result of azimuth ambiguity suppression, and the calculation results of azimuth ambiguity ratio are listed in Table IV. It can be seen from the visual effect and the measurement results of azimuth ambiguity ratio that the processing results of this method are good.

As mentioned in Section III-B, this method has its applicable scenarios, along with some shortcomings. In fact, missing detection will indeed make ambiguity suppression unable to achieve

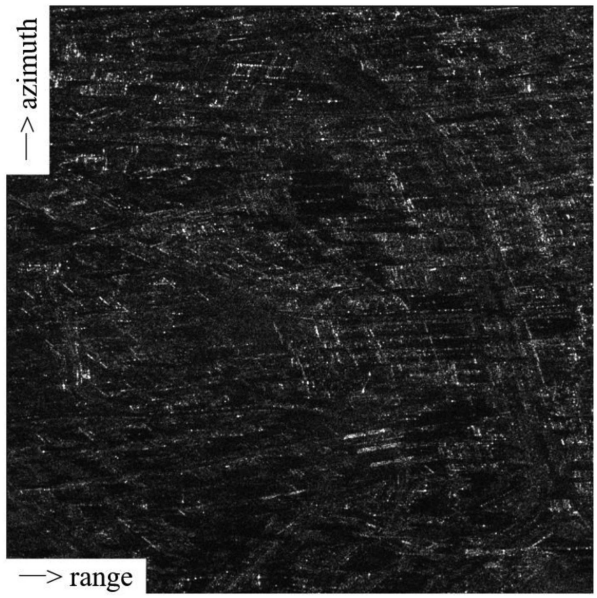

Fig. 21. Ambiguity suppression result of Fig. 19.

TABLE IV
RESULTS OF AZIMUTH AMBIGUITY SUPPRESSION

item	Raw image	Method of this article
Ambiguity ratio (dB)	-9.5432	-25.4615
Ambiguity area average energy (dB)	21.4488	5.5305

TABLE V
PARAMETERS OF RADARSAT IMAGE

parameter	value
PRF	1100.079 Hz
PRF_{im}	2200.158 Hz
Reference velocity	7192.3 m/s
Reference slant range	850.072 km
Bandwidth	50 MHz
Sample rate	56.3 MHz

TABLE VI
RESULTS OF AZIMUTH AMBIGUITY SUPPRESSION

item	order	Raw image	Method of this article
Ambiguity ratio (dB)	First-order	-24.9277	-42.6456
Ambiguity area average energy (dB)		68.3915	50.6736
Ambiguity ratio (dB)	Second-order	-28.9159	-43.0363
Ambiguity area average energy (dB)		64.4033	50.2829

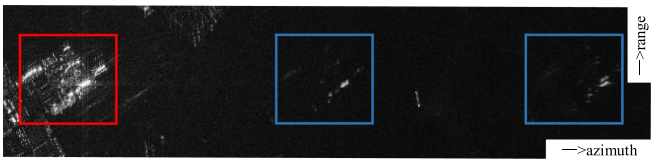

Fig. 22. Original image result of Radar-Sat taken in Qingdao in strip mode.

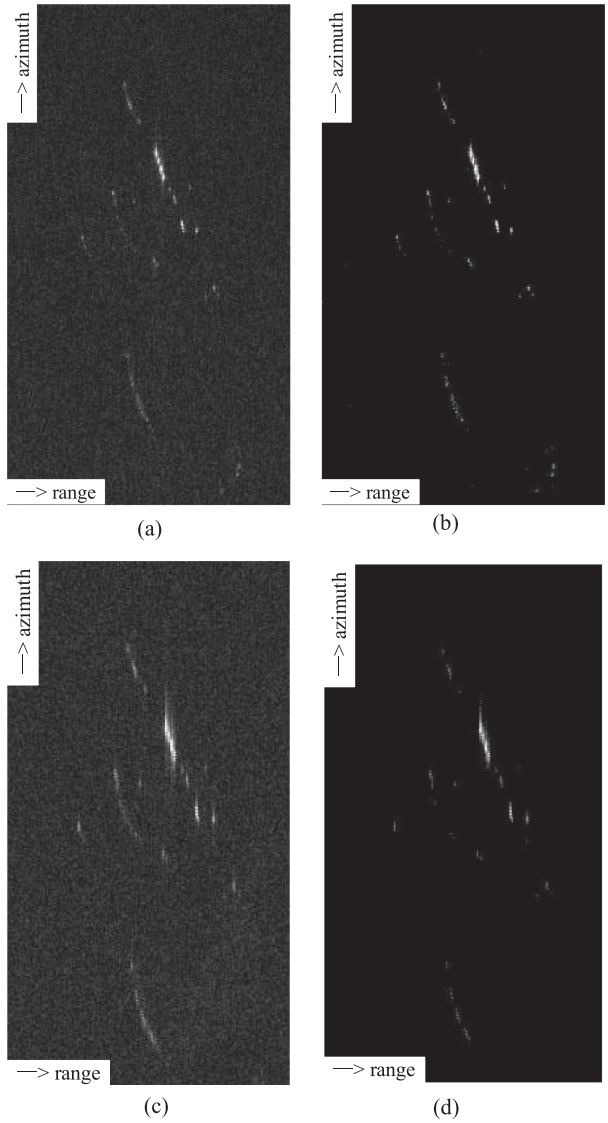

Fig. 23. Focusing and detecting results of the ambiguity area for slice data of Radar-Sat taken in Qingdao. (a) First-order ambiguity area focusing result. (b) Detection result of (a). (c) Second-order ambiguity area focusing result. (d) detection result of (c).

the effect completely invisible to the naked eye, but it is indeed a great improvement compared with the original image. False detection will indeed suppress the energy of the target in the main area, so we set the threshold higher for the data with complex background which can reduce the false detection rate to a certain extent. A small amount of false detection will cause some targets to lose energy and then cause the phenomenon of roof cutting. This is indeed the shortcoming of this method, and it will be improved in the future.

In order not to affect the target in the main area to the greatest extent, we set a higher threshold, so that some azimuth ambiguity with low energy are not suppressed, which is the result of judge and weigh.

C. Processing Results of Pure Background

We found multiorder azimuth ambiguity in the satellite image of Radar-Sat which is dual-channel strip mode. The specific parameters are shown in Table V .

The original image scene is too large with little azimuth ambiguity, so we only intercept the positions where there is multiorder azimuth ambiguity, as shown in Fig. 22. In the figure, we can see the main area target circled in the red box and the multiorder azimuth ambiguity circled in the blue box.

We get the imaging results of the first-order and second-order ambiguity areas as shown in Fig. 23(a) and (c), and the corresponding detection results are shown in Fig. 23(b) and (d). The detection rate of $+1$ order is 99.1% and the false detection rate is 0.9%. The detection rate of the -1 order is 98.9%, and the false detection rate is 1.6%. It can be seen that the strong points belonging to the targets in the ambiguity area are basically detected.

The results of ambiguity suppression are shown in Fig. 24. Through visual comparison, we can see that the azimuth ambiguity suppression effect is obvious. We selected the main area target in the red box and the corresponding ambiguity area target to calculate the ambiguity ratio, and the results are listed in Table VI. We also calculated the energy of the ambiguity area in the original image and ambiguity suppression results, and the

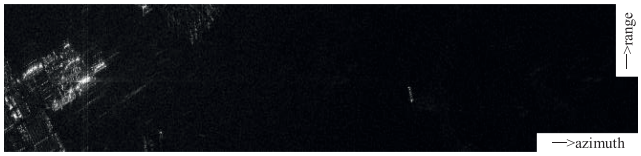

Fig. 24. Ambiguity suppression result of Fig. 22.

results are listed in Table VI. It can be seen from the results that the azimuth ambiguity ratio and the energy value of the ambiguity area both decreases. This shows the feasibility of this method.

V. Conclusion

In this article, an azimuth ambiguity suppression method based on ambiguity area imaging and detection is proposed, which is suitable for strip, spotlight and mulichannel mode. This method can remove most of the azimuth ambiguity while maintaining the quality of the original image to the greatest extent which are proved by the processing results of the real satellite data. It is a good auxiliary processing help for SAR systems with serious azimuth ambiguity.

References

[1] Z. Yongjun and L. Caiping, "Ambiguity analysis of synthetic aperture radar," *J. Electron. Inf.*, vol. 26, no. 9, pp. 1455–1460, 2004.
[2] H. Wei et al., "An improved azimuth ambiguity suppression method of ideal filter," *Electron. Meas. Technol.*, vol. 5, pp. 25–29, 2011.
[3] A. M. Guarnieri, "Adaptive removal of azimuth ambiguities in SAR images," *IEEE Trans. Geosci. Remote Sens.*, vol. 43, no. 3, pp. 625–633, Mar. 2005.
[4] W. Zhengsheng et al., "An improved azimuth ambiguity suppression method for SAR images," *Surveying Mapping Bull.*, vol. 1, pp. 149–152, 2014.
[5] X. Peng et al., "A SAR image azimuth ambiguity suppression method based on compressed sensing restoration algorithm," *J. Radar*, vol. 5, no. 1, pp. 39–45, 2016.
[6] G. Di Martino, A. Iodice, D. Riccio, and G. Ruello, "Filtering of azimuth ambiguity in stripmap synthetic aperture radar images," *IEEE J. Sel. Topics Appl. Earth Observ. Remote Sens.*, vol. 7, no. 9, pp. 3967–3978, Sep. 2017.
[7] Y. Wu, Z. Yu, P. Xiao, and C. Li, "Azimuth ambiguity suppression based on minimum mean square error estimation," in *Proc. IEEE Geosci. Remote Sens. Symp.*, 2015, pp. 2425–2428.
[8] Y. Wu, Z. Yu, P. Xiao, and C. Li, "Suppression of azimuth ambiguities in spaceborne SAR images using spectral selection and extrapolation," *IEEE Trans. Geosci. Remote Sens.*, vol. 56, no. 10, pp. 6134–6147, Oct. 2018.
[9] N. Oishi and K. Suwa, "Azimuth ambiguity detection and suppression in SAR images," in *Proc. IEEE Int. Geosci. Remote Sens. Symp.*, 2019, pp. 676–679.
[10] X. Hui et al., "Study on azimuth ambiguity of spaceborne SAR," *Fire Control Radar Technol.*, vol. 40, no. 2. pp. 1–5, 2011.
[11] K. Deliang, S. Hongjun, and Z. Minhui, "Azimuth ambiguity analysis and simulation of declination spotlight SAR," *J. Test Technol.*, vol. no. 4, pp. 62–66, 2007.
[12] C. Zengju, S. Hongjun, and X. Haisheng, "Azimuth ambiguity analysis of stripping sliding spotlight mode SAR," *Sci., Technol. Eng.*, vol. 11, pp. 2215–2219, 2011.
[13] Y. Wang, Z. Ding, P. Xu, K. Chen, T. Zeng, and T. Long, "Strip layering diagram-based optimum continuously varying pulse interval sequence design for extremely high-resolution spaceborne sliding spotlight SAR," *IEEE Trans. Geosci. Remote Sens.*, vol. 59, no. 8, pp. 6751–6770, Aug. 2021.
[14] M. Villano and G. Krieger, "Spectral-based estimation of the local azimuth ambiguity-to-signal ratio in SAR images," *IEEE Trans. Geosci. Remote Sens.*, vol. 52, no. 5, pp. 2304–2313, May 2014.

Wen Xuejiao was born in Jilin, China. She received the B.S. degree in electronic engineering from Shanghai Jiaotong University, Shanghai, China, in 2014, and the M.S. degree in signal processing and information science from the University of Chinese Academy of Sciences, Beijing, China, in 2017.

She is currently an Associate Researcher with Key Laboratory of Spatial Information Intelligent Processing System, Suzhou Aerospace Information Research Institute. Her current research interests include signal processing and moving target processing technology with advanced SAR.

Qiu Xiaolan (Senior Member, IEEE) was born in 1982. She received the B.S. degree in electronic engineering and information science from the University of Science and Technology of China, Hefei, China, in 2004, and the Ph.D. degree in signal and information processing from the Graduate University of Chinese Academy of Sciences, Beijing, China, in 2009.

Since 2009, she has been with the Aerospace Information Research Institute, Chinese Academy of Sciences, Beijing. Since 2020, she has also been with the Suzhou Aerospace Information Research Institute, Suzhou, China. Her research interests include synthetic aperture radar (SAR) 2-D/3-D imaging and microwave vision. She is the Senior Member of IEEE. She was funded by the Excellent Young Scienctists Fund of NSFC. She serves as the Associate Editor of IEEE Geoscience and Remote Sensing Letters and Young Associate Editor of *Journal of Radars*.

Cui Lei was born in Gansu Province. He received the B.S. degree in communication engineering from the Beijing University of Technology, Beijing, China, in 2013, and the M.S. degree in signal processing from the Beijing University of Technology, in 2016.

He is currently an Associate Researcher with Key Laboratory of Spatial Information Intelligent Processing System, Suzhou Aerospace Information Research Institute. His current research interest is SAR data preprocessing.

Wang Jiyun is currently working toward the Master's degree with Suzhou University, Suzhou, China.

His current research interest focuses on SAR data processing.

Chen Qi received the M.S. and Ph.D. degrees in signal processing and information science from the Graduate University of Chinese Academy of Sciences, Beijing, China, in 2004 and 2007, respectively.

He is the Director of GF-3 satellite ground data processing system. His current research interest focuses on high resolution SAR data processing technology.